# Structural basis for endosomal trafficking of diverse transmembrane cargos by PX-FERM proteins

Rajesh Ghai[a], Andrea Bugarcic[a,1], Huadong Liu[b,c,1], Suzanne J. Norwood[a,1], Sune Skeldal[d], Elizabeth J. Coulson[d], Shawn Shun-Cheng Li[b,c], Rohan D. Teasdale[a], and Brett M. Collins[a,2]

[a]Institute for Molecular Bioscience and [d]Queensland Brain Institute, The University of Queensland, St. Lucia, QLD 4072, Australia; and [b]Department of Biochemistry and [c]Siebens Drake Medical Research Institute, University of Western Ontario, London, ON, Canada N6A 5C1

Edited by K. Christopher Garcia, Stanford University, Stanford, CA, and approved December 31, 2012 (received for review September 20, 2012)

**Transit of proteins through the endosomal organelle following endocytosis is critical for regulating the homeostasis of cell-surface proteins and controlling signal transduction pathways. However, the mechanisms that control these membrane-transport processes are poorly understood. The Phox-homology (PX) domain-containing proteins sorting nexin (SNX) 17, SNX27, and SNX31 have emerged recently as key regulators of endosomal recycling and bind conserved Asn-Pro-Xaa-Tyr–sorting signals in transmembrane cargos via an atypical band, 4.1/ezrin/radixin/moesin (FERM) domain. Here we present the crystal structure of the SNX17 FERM domain bound to the sorting motif of the P-selectin adhesion protein, revealing both the architecture of the atypical FERM domain and the molecular basis for recognition of these essential sorting sequences. We further show that the PX-FERM proteins share a promiscuous ability to bind a wide array of putative cargo molecules, including receptor tyrosine kinases, and propose a model for their coordinated molecular interactions with membrane, cargo, and regulatory proteins.**

endosome | protein crystallography | X-ray scattering | membrane trafficking

The cell-surface levels of signaling and adhesion receptors, nutrient transporters, ion channels, and many other proteins are tightly regulated by opposing endocytic, exocytic, and endosomal recycling transport pathways. The selective sorting of these transmembrane proteins is the consequence of their interaction with essential adaptor proteins via conserved motifs present in their cytosolic tails, generally based on short linear amino acid sequences such as the Yxxϕ, DxxLL, and [DE]xxxL[LI] motifs (where ϕ is any bulky hydrophobic side-chain, and x is any residue) recognized by clathrin adaptors (1–3). The first identified sorting signal was the Asn-Pro-Xaa-Tyr (NPxY) motif, initially described in the LDL receptor (LDLR) isolated from patients suffering from familial hypercholesterolemia, where mutation of the sequence results in defective internalization and cholesterol uptake (4). The recent structure of the autosomal recessive hypercholesterolemia protein (ARH) phosphotyrosine-binding (PTB) domain in complex with the LDLR intracellular domain (ICD) provides the molecular basis of LDLR recognition and internalization within clathrin-coated pits by endocytic adaptor proteins (5).

Although little is known about the sorting sequences and mechanisms required for competing endosome-to-cell surface recycling pathways, emerging evidence shows that the NPxY motif not only is vital to internalization but also aids cargo recycling via organelle-specific recognition by the endosomal protein, sorting nexin 17 (SNX17). SNX17 is a member of the Phox-homology (PX) domain-containing protein family and has been shown to be a critical regulator of endosomal sorting and cell-surface recycling of several essential cargo molecules. These include P-selectin (6–8), amyloid precursor protein (APP) (9, 10), integrins (11, 12), and members of the LDL receptor family (13–17) via recognition of an NPxY or alternative NxxY signal. The PX proteins [often called "sorting nexins" (SNXs)] are a large family of molecules that govern diverse endosomal trafficking and signaling processes and, by definition, possess a phosphoinositide lipid-binding PX domain that promotes membrane recruitment (18–20).

We recently showed that, together with SNX27 and SNX31, SNX17 is a member of the PX-band 4.1/ezrin/radixin/moesin (FERM) subfamily of endosomal proteins (9). These molecules possess an N-terminal phosphatidylinositol-3-phosphate (PI3P)-binding PX domain that mediates localization to the early endosome and an atypical C-terminal FERM domain responsible for binding the NPxY/NxxY sequence for recycling (9). Although no specific function has been assigned to SNX31, a recent study revealed that mutations in the protein lead to melanoma (21). SNX27 is unique within the PX family, containing an N-terminal postsynaptic density 95/discs large/zonula occludens-1 (PDZ) domain that binds PDZ-binding motif (PDZbm)-containing cargo such as the β2-adrenergic receptor to influence alternative cargo recycling (18–20, 22–26). Thus a consensus is emerging that PX-FERM proteins are key regulators of endosome-to-cell surface recycling by binding PDZbm and/or NPxY/NxxY recycling signals. Recently the structure of the SNX27 PDZ domain bound to the PDZbm of the Kir3.3 potassium channel was determined, defining the mechanism of cargo recruitment through this interaction (25). However, there is no structural information on the atypical FERM domain of these proteins, and the molecular mechanism underlying recognition of the NPxY/NxxY recycling signal is still unknown.

Here we present the crystal structure of the atypical FERM domain of SNX17 in complex with an NPxY/NxxY sorting sequence from the ICD of the recycling cargo P-selectin, showing the mechanism underpinning endosome-to-cell surface sorting by the PX-FERM family. Using peptide arrays, we further identify a large pool of transmembrane proteins harboring NPxY/NxxY sequences as putative cargos for the PX-FERM proteins, prominent among which are many members of the receptor tyrosine kinase (RTK) protein family, and observe a significant bias of SNX27 toward phosphorylated peptides, suggesting this protein may interact preferentially with stimulated receptors. Together, our data show that PX-FERM proteins share a promiscuous binding mechanism for interacting with cargos containing an NPxY/NxxY motif. Finally, we propose a model, based

Author contributions: R.G., R.D.T., and B.M.C. designed research; R.G., A.B., S.J.N., S.S., and B.M.C. performed research; H.L., E.J.C., and S.S.-C.L. contributed new reagents/analytic tools; R.G., A.B., H.L., S.J.N., S.S., E.J.C., S.S.-C.L., R.D.T., and B.M.C. analyzed data; and R.G., A.B., H.L., S.J.N., S.S., R.D.T., and B.M.C. wrote the paper.

The authors declare no conflict of interest.

This article is a PNAS Direct Submission.

Data deposition: Crystallography, atomic coordinates, and structure factors have been deposited in the Research Collaboratory for Structural Bioinformatics Protein Data Bank (RCSB PDB) database, http://www.rcsb.org (RCSB PDB ID 4GXB).

[1]A.B., H.L., and S.J.N. contributed equally to this work.

[2]To whom correspondence should be addressed. E-mail: b.collins@imb.uq.edu.au.

See Author Summary on page 2707 (volume 110, number 8).

This article contains supporting information online at www.pnas.org/lookup/suppl/doi:10.1073/pnas.1216229110/-/DCSupplemental.

on low-resolution small-angle X-ray scattering (SAXS) data, for coincident membrane and cargo recognition by the PX-FERM proteins required for organelle-specific trafficking.

## Results

**Crystal Structure of the Atypical FERM Domain of SNX17.** Based on the previous report that SNX17, SNX27, and SNX31 contain an atypical FERM domain that recognizes NPxY/NxxY cargo (9), we set out to address two questions: the overall structure of the atypical FERM domain and the molecular mechanism underpinning recognition of the NPxY/NxxY motif. Because initial attempts to crystallize the SNX17 FERM domain failed, we also screened a number of SNX17 constructs fused with the ICDs of several NPxY/NxxY cargos separated by a short linker (Fig. S1). This process led to the formation of diffraction-quality crystals of the SNX17 FERM domain fused with the P-selectin ICD. The structure of the SNX17 FERM domain/P-selectin ICD complex was solved by single isomorphous replacement with anomalous scattering (SIRAS) and refined to a resolution of 1.8 Å (Table S1).

The structure of the complex is discussed further below; here we focus on the unique features of the atypical SNX17 FERM domain. Although the SNX17 FERM domain shares a very low (<15%) sequence identity with prototype FERM domains (27–29), it comprises three analogous submodules, F1, F2, and F3 (Fig. 1 and Fig. S2). Consistent with our previous predictions, the F1 lobe has a ubiquitin-like fold and resembles a Ras-association (RA) domain, F2 is a small helical bundle, and F3 is structurally related to the PTB and pleckstrin homology (PH) domains (9). The SNX17 FERM domain has an extended loop between β5C and β6C in the F3 lobe that has low electron density, indicating that it is structurally flexible. Secondary structure predictions indicate that this loop is present in SNX31 but not in SNX27 (NPxY), and other canonical FERM domain proteins do not possess this flexible region.

We next compared the SNX17 FERM domain by superposition with the canonical FERM domains of radixin (Fig. 1*B*) (28) and talin (27). The radixin and talin (in F2 and F3 only) FERM domains show an overall rmsd of 2.9 Å over 214 Cα atoms and 3.0 Å over 129 Cα atoms, respectively. SNX17 shares the conserved submodules F1 and F3 and has an overall architecture that most closely resembles the classical radixin-like FERM cloverleaf structure. This structure is in direct contrast to the linear and elongated FERM domain of the talin protein (27). Most importantly, the SNX17 FERM domain has a distinctive, short F2 subdomain lacking the typical α3B helix and extended loop region, resulting in a total of three helices instead of four. For consistency with canonical FERM structures, we refer to the first two F2 helices of SNX17 as "α1B" and" α2B" and to the third helix as "α4B" rather than α3B. This truncation of the helical bundle of the F2 module is a unique feature of the PX-FERM proteins and has not been found in any other FERM domains studied to date.

**Crystal Structure of the SNX17 FERM Domain Resembles the SNX17 and SNX27 Solution Conformations.** Except for talin, all FERM domain structures have been found to possess a similar cloverleaf architecture; talin, in contrast, has an unconventional linear arrangement of the F1-F2-F3 modules (27). We used SAXS to confirm that the crystalline structure of the SNX17 FERM domain is representative of its solution state and in parallel compared this

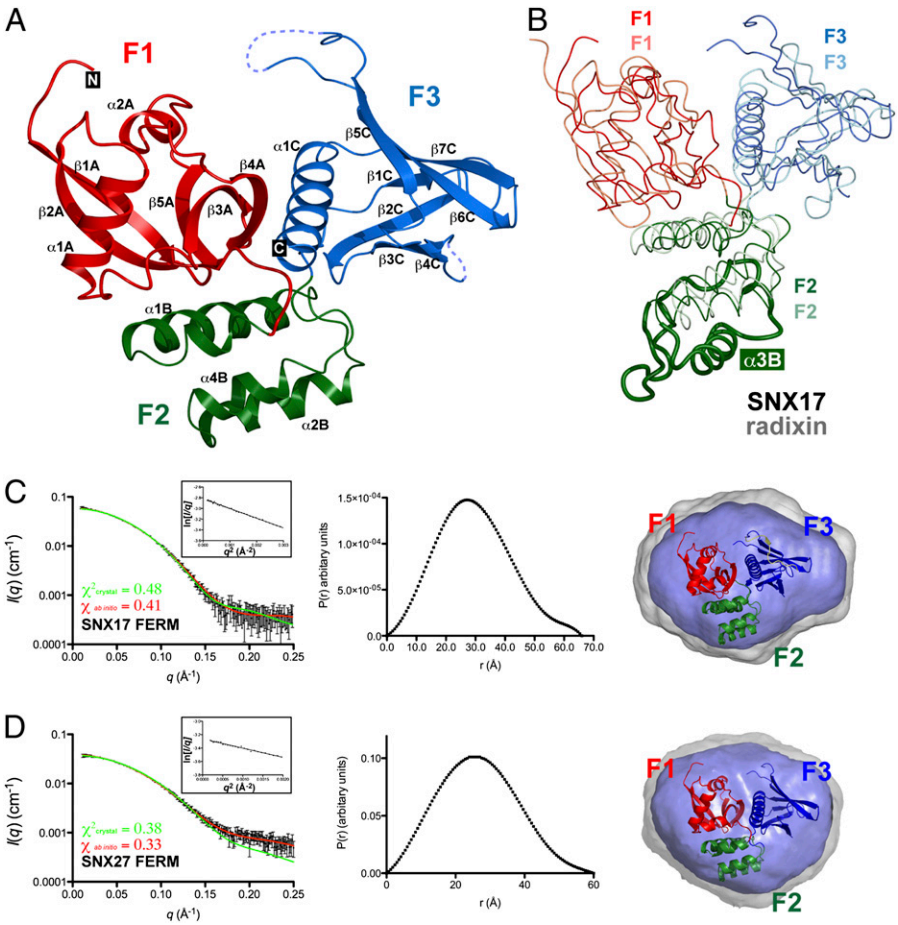


**Fig. 1.** Structure of the atypical SNX17 FERM domain. (*A*) Ribbon representation of the atypical SNX17 FERM domain crystal structure depicting the three submodules F1, F2, and F3 in red, green, and blue, respectively. (*B*) Overlay of the FERM domain of SNX17 with radixin [Protein Data Bank (PDB) ID, 1GC7)] (28). Brighter worms show SNX17; paler colors indicate radixin. The α3B helix, present in all other FERM domains but absent in SNX17, SNX27, and SNX31, is indicated by thicker green worms. The cloverleaf arrangement of the three submodules of SNX17 shows overall similarity to radixin but differs dramatically from the extended conformation of the talin protein (27). (*C* and *D*) Solution SAXS data are shown for SNX17 (*C*) and SNX27 (*D*) FERM domains. Both SNX17 and SNX27 FERM domains adopt compact, globular structures in solution, consistent with the SNX17 FERM domain crystal structure. (*Left*) Experimental SAXS profiles in black overlaid with the theoretical profiles calculated from the SNX17 crystal structure by CRYSOL (green) or the ab initio model determined by the program GASBOR (red). *Insets* show the Guinier plots for the experimental data. (*Center*) *P(r)* functions derived from the SAXS data. (*Right*) Averaged (gray) and filtered (blue) structural envelopes from GASBOR. The crystal structure of the SNX17 FERM domain is shown in ribbon representation and was docked into the ab initio envelopes using SUPCOMB20.

structure with the solution structure of the SNX27 FERM domain. Multiangle laser light scattering (MALLS) data reveal that the FERM domains of both SNX17 (fused to P-selectin) and SNX27 are monomeric and monodispersed in solution (Fig. S3). Scattering curves for both proteins together with theoretical scattering profiles calculated from the ab initio models with the lowest $\chi$ values are shown in Fig. 1 *C* and *D*. The pair distribution functions, $P(r)$, also are shown in Fig. 1, and the derived structural parameters for these proteins are presented in Table S2.

The scattering profiles of both SNX17 and SNX27 FERM domains determined by SAXS are in excellent agreement with the theoretical scattering curve calculated by CRYSOL from the crystal structure of the SNX17 FERM domain, with low $\chi^2$ values of 0.48 and 0.38, respectively (Fig. 1 *C* and *D*). This agreement confirms that the solution structures of the SNX17 and SNX27 FERM domains are highly similar to each other and that both closely resemble the SNX17 crystal structure. Visual comparisons of the SNX17 FERM domain crystal structure with the ab initio envelopes calculated from the SAXS data also show close agreement, confirming that both the SNX17 and SNX27 FERM domains have a compact solution structure consistent with the crystalline conformation and distinct from that of the extended talin FERM domain (27).

**Mechanism of NPxY/NxxY Cargo Recognition by the SNX17 Atypical FERM Domain.** SNX17 has been shown to control the endosomal transport and recycling of transmembrane cargo via the recognition of NPxY/NxxY sequences present in their tail regions, but the structural basis for this transport remains unknown. Identified cargos include P-selectin, APP, members of LDLR family, and integrins (Fig. 2*A*). To determine the mechanism of cargo recognition by the PX-FERM proteins, the structure of the SNX17 FERM domain in complex with the entire P-selectin ICD was resolved by X-ray crystallography (Fig. 2). To obtain a stable complex, the P-selectin ICD was genetically fused to the C terminus of SNX17 (Fig. S1). The residues of P-selectin observed in this crystal structure were $^{753}$GTYGVFTNAAYDPT$^{766}$, and no electron density was seen for the linker or N-terminal region of the P-selectin ICD preceding this bound peptide. In further discussions Tyr763 is designated "$Y_0$," and other residues are numbered with respect to this designation (e.g., Asn760 is $N_{-3}$).

The structure reveals that SNX17 associates specifically with the NPxY/NxxY motif within the P-selectin ICD via the F3 module of its FERM domain (Fig. 2*B*), which structurally resembles the insulin receptor substrate-1 class of PTB domain (30, 31). The peptide binds via β augmentation in the complementary groove provided by α1C and β5C of SNX17 and forms a number of hydrogen bonds together with hydrophobic and main chain–main chain contacts (Fig. 2 *C* and *D*). The P-selectin ICD buries a solvent accessible surface area of 1,102 Å$^2$ as calculated by the PISA server (www.ebi.ac.uk) (32).

Both the $N_{-3}$ and $Y_0$ residues of the core NPxY/NxxY motif are critical for SNX17 interaction (6, 9–11, 15, 16, 33, 34). The critical $Y_0$ residue of the core NAAY sequence of P-selectin stacks between Arg319 and Leu353 of β5C of SNX17 and $P_2$ of the peptide (Fig. 2*D*). The $A_{-1}$ and $A_{-2}$ residues lie within the pocket formed by Ala380 and Met384 within SNX17 helix α1C. The strictly conserved $N_{-3}$ (Asn760 of P-selectin) establishes a number of hydrogen bonds and extends into a deep pocket, making contacts with the backbone carbonyl of SNX17 Val315. Bridging by water molecules facilitates several hydrogen bonds, and, critically, the upstream $F_{-5}$ of the peptide is involved in a stacking interaction with SNX17 Trp321. Indeed in P-selectin the $F_{-5}$ residue is important for SNX17 interaction (6), and the similar residues $Y_{-5}$ in APP (10) and $I_{-5}$ in LRP1 (15) also contribute to binding, suggesting that aromatic or bulky hydrophobic side chains at the −5 position impart an additional sequence specificity. Further contacts are made by peptide residue $Y_{-8}$ with SNX17 Ser325, facilitated by a bridging water molecule. Analysis of the FERM domains of SNX17, SNX27, and SNX31 proteins using the ConSurf Server (http://consurf.tau.ac.il) (35) shows that the peptide-binding groove in the F3 lobe is highly conserved among all PX-FERM proteins (Fig. 2*E*), indicating that other PX-FERM proteins share the same fundamental mechanism for binding NPxY/NxxY cargo motifs.

A recent report by Böttcher et al. (12) showed that double mutation of Gln360 and Trp361 side chains in SNX17 (Q360A/W361A) abrogates interaction with β1 integrin; however, our crystal structure reveals that these residues in the β7C strand do not contribute directly to the peptide-binding groove formed by strand β5C and helix α1C. Gln360 is remote and is oriented away from the peptide site. Trp361 also is remote from the peptide-binding groove but does stabilize SNX17 residue Arg322 in the adjacent β5C strand that in turn contributes directly to the binding site, perhaps explaining why its mutation affects β1 integrin interaction. This double mutation thus may lead to localized instability in the binding pocket that inhibits association.

The structure of the NPxY/NxxY complex with the PTB-like F3 subdomain of SNX17 is similar to the complexes of several other proteins with related PTB domain structures (Fig. 3 *A* and *B*). Comparison of the SNX17 FERM domain/P-selectin ICD structure with the PTB domain of FE65/APP ICD complex (36), the ARH/LDLR ICD complex (5), and the Talin (F2-F3)/β1D integrin ICD complex (37) reveals that the orientation of the critical $N_{-3}$ and $Y_0$ from the NPxY/NxxY motifs of APP, LDLR, and β1D integrin is similar to that of the analogous residues from the P-selectin ICD. Although SNX17 is only distantly related to these other proteins, it appears that the NPxY/NxxY motif of P-selectin binds SNX17 F3 via a similar mechanism.

**Overlapping Trafficking Motifs Are Present in the P-Selectin ICD.** In addition to the NPxY/NxxY SNX17-binding signal, the ICD of P-selectin also contains an overlapping Yxxϕ motif ($^{755}$YGVF$^{758}$ in P-selectin) recognized by the activating protein 2 (AP2) clathrin adaptor for endocytosis, presenting an interesting example of how overlapping sorting sequences can be used by different trafficking machineries. The structure of the AP2 μ2 subunit in complex with the P-selectin YGVF peptide has been determined by X-ray crystallography (38), allowing a comparison with the SNX17-bound P-selectin ICD containing both trafficking signals (GTYGVFTNAAYDPT) to investigate any similarities in the peptide-binding mechanisms (Fig. 3*C*). The overlay of the YGVF internalization signal from the two P-selectin peptides shows that the aromatic side chains are in similar relative orientations, and in each case the peptides make similar β-augmentation interactions. However, the overall peptide conformations differ significantly, and the two motifs are recognized in distinct ways, as would be expected from the different structural scaffolds of the SNX17 and μ2 adaptors.

**Mutational Analysis Confirms the NPxY/NxxY Cargo-Binding Mechanism.** To confirm the molecular determinants that dictate the association between SNX17 and NPxY/NxxY cargo, a number of mutations were introduced into the αβ-binding groove of the F3 region of SNX17 (Fig. S2). We then performed GST pull-down assays using the GST-tagged P-selectin ICD and His-tagged wild-type SNX17 or SNX17 mutants R319D, W321A, A380D, and M384. As shown in Fig. 4*B*, the W321A and A380D mutations completely inhibit the interaction. The R319D and M384E mutations show reduced interactions. We also tested the binding of these mutants to a synthetic peptide from P-selectin (GTYGVFTNAAYDP) using isothermal titration calorimetry (ITC). The titration of wild-type SNX17 with the peptide generated significant binding heat signals, and the $K_d$ was estimated from the binding curve to be 2.7 μM (Fig. 4*B* and Table S3). The mutants L353W, A380D, and M384E reduced the binding affinity by approximately

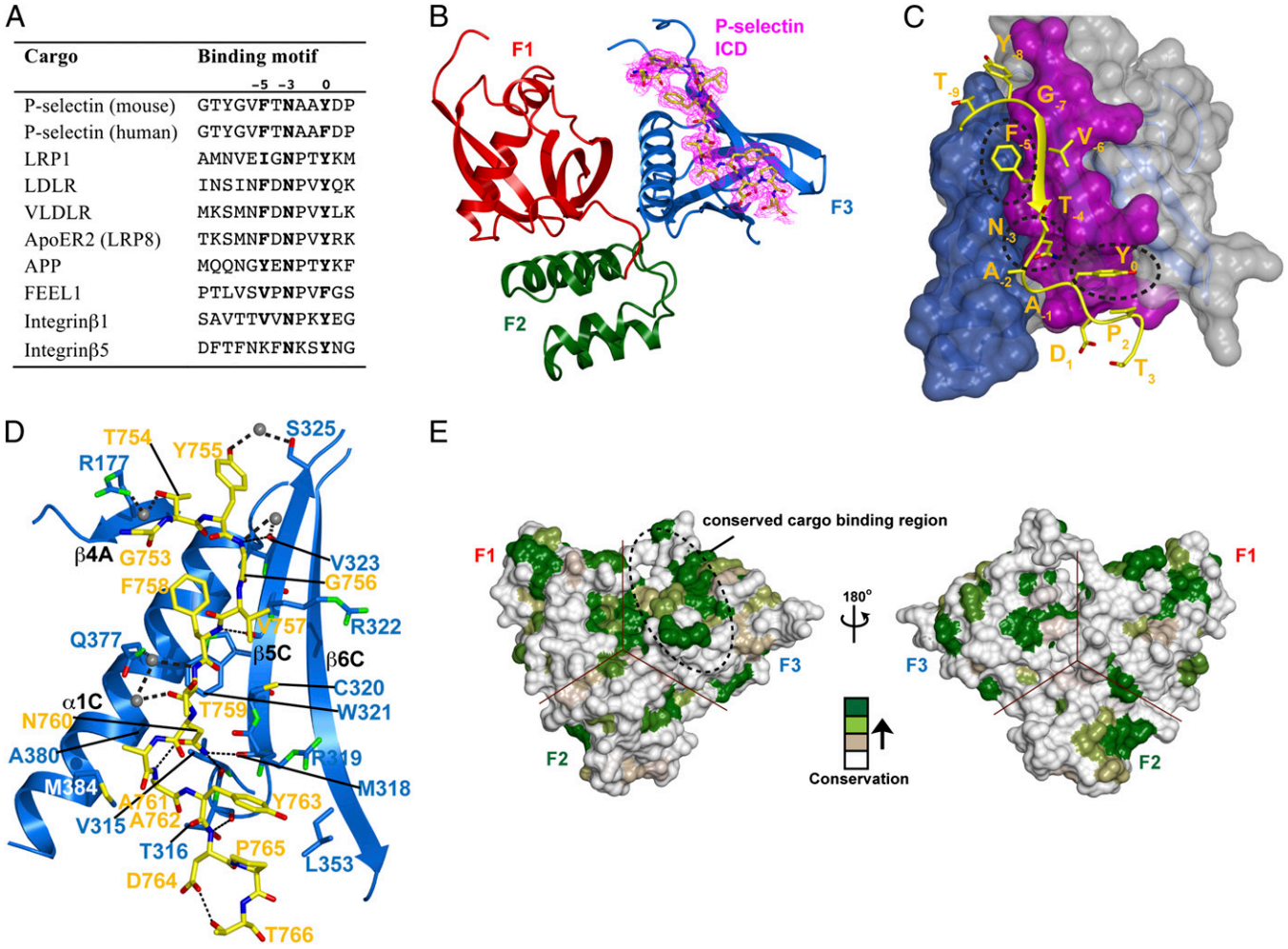


**Fig. 2.** Structure of the SNX17 FERM domain in complex with the P-selectin ICD. (*A*) Table of NPxY/NxxY sequences from cargo ICDs previously found to interact with SNX17. Surrounding sequences from the ICDs are shown. See text for references. (*B*) The crystal structure of the SNX17 FERM domain bound to the P-selectin ICD shows that the NPxY/NxxY motif binds the F3 submodule of SNX17. The P-selectin peptide is shown in yellow stick representation, and refined $2F_o$-$F_c$ electron density contoured at 1.5σ for the bound peptide is shown in magenta. (*C*) Surface representation of the P-selectin ICD-binding groove formed by the SNX17 helix α1C (blue) and strand β5C (magenta). The peptide residues that form critical contacts with the β5C-α1C groove are indicated by dashed circles. (*D*) Detailed view of the interaction between the F3 lobe of SNX17 and the ICD of P-selectin. The P-selectin peptide is shown in explicit atomic model (yellow cylinders), and the F3 module is represented as ribbons. The amino acids of the SNX17 F3 domain that are involved in the interaction with the P-selectin ICD are shown as blue cylinders, and hydrogen bonds are depicted by dashed lines. Interfacial water molecules are shown as gray spheres. (*E*) Mapping residues that are conserved among SNX17, SNX27, and SNX31 PX-FERM proteins onto the SNX17 structure highlights the conservation of the peptide-binding site. The surface of the SNX17 FERM domain colored white (nonconserved) to green (highly conserved). The dashed ellipse indicates the peptide-binding groove.

5-, 10-, and 20-fold respectively; the binding of the W321A mutant was too low to be determined.

To confirm that the APP NPxY/NxxY motif interacts with SNX17 in a similar manner to P-selectin, we similarly tested the binding of the APP peptide (CKQNGYENPTYKFFE) to wild-type and mutant SNX17 proteins using ITC. SNX17 binds the APP peptide with a $K_d$ of 22 μM, consistent with our previous reports (9), but the M384E mutant binds only weakly (Fig. 4*B*). The mutants L353W, A380D, and W321A completely abolish the interaction. These data confirm that SNX17 interacts with different NPxY/NxxY motif-containing cargo in an identical manner.

**SNX27 Shares a Conserved NPxY/NxxY-Binding Site with SNX17.** Previously we showed that SNX27, like SNX17, has the ability to interact with the APP NPxY/NxxY motif (9). Using GST pull-downs, we also were able to observe a direct interaction of P-selectin and APP with SNX27, demonstrating a conserved NPxY/NxxY-binding propensity for members of the PX-FERM family (Fig. 4*C*). To confirm that the interaction occurs via the same mechanism, we designed mutants in the F3 region of SNX27 based on structure-based sequence alignments (Fig. S2). W475A and K520Q mutations occur at sites analogous to the W321A and M384E mutations in SNX17, respectively. GST pull-down experiments using the GST-tagged P-selectin and APP cytoplasmic tails show that both mutations abrogate the binding with the P-selectin and APP ICD and confirm that PX-FERM proteins possess a conserved binding site for recognition of NPxY/NxxY cargo.

**NPxY/NxxY-Binding Site of SNX17 Is Required for Membrane Localization.** Previous studies suggest an essential role for coincidence detection of both phosphoinositides and cargo for membrane localization of many trafficking coat proteins (39); examples include the clathrin adaptor complex AP2 regulating endocytosis (40) and the GGA proteins regulating Golgi trafficking (41). We have shown that the PI3P-binding site of the SNX17 PX domain is required for endosomal membrane recruitment of the protein (9), and the same has been demonstrated for SNX27 (24). We next tested whether the NPxY/NxxY

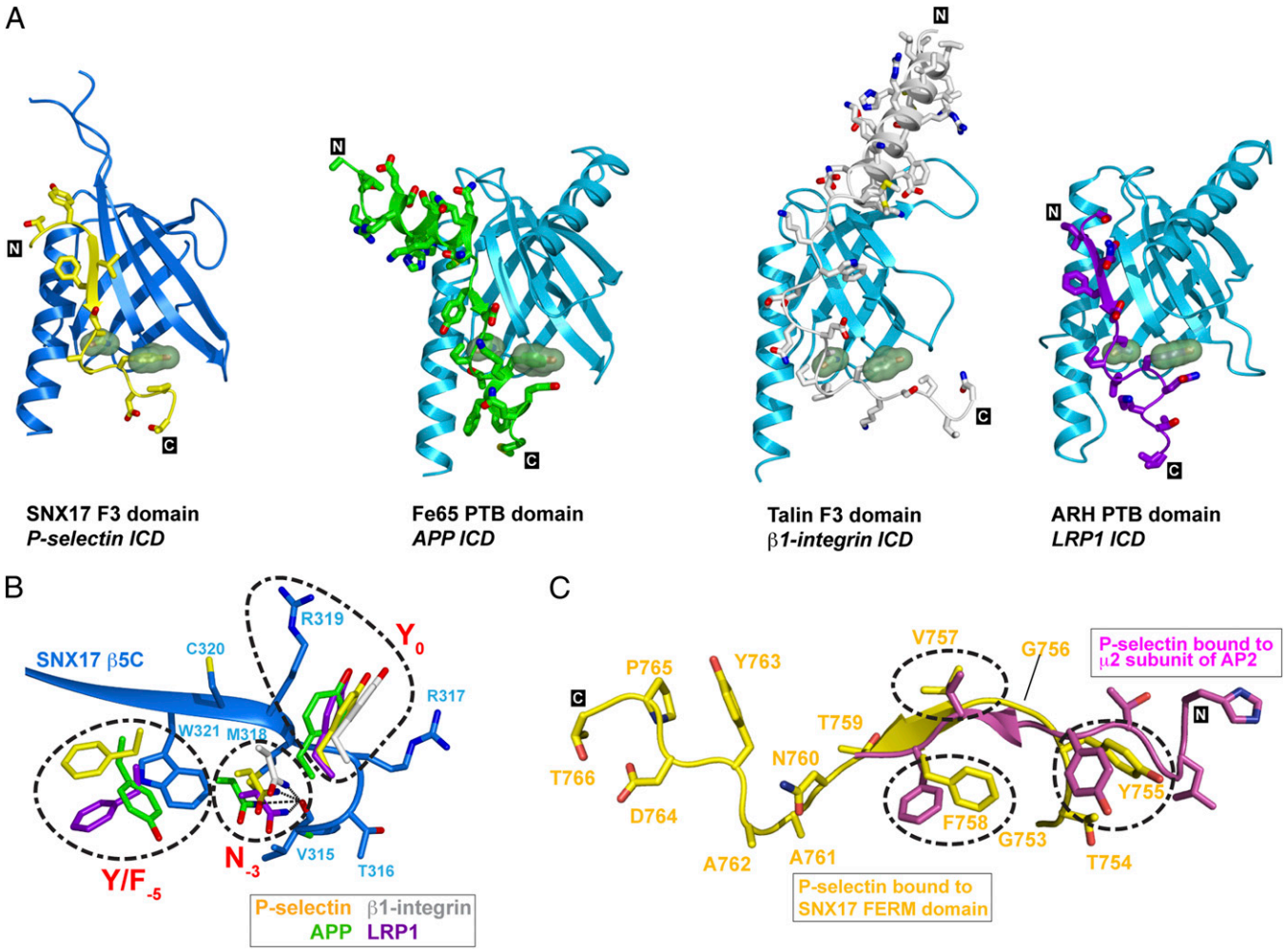


**Fig. 3.** Comparison of the SNX17/P-selectin complex with distantly related endocytic and signaling complexes. (*A*) The SNX17 F3 module is shown in blue bound to P-selectin ICD, shown in yellow, and the critical $N_{-3}$ and $Y_0$ of the NPxY/NxxY motif are highlighted in surface representation. The structure is similar to several other endocytic and signaling complexes that are shown for comparison: the PTB domain of FE65 bound to the APP ICD (PDB ID, 3DXC) (36, 56), the F3 subdomain of talin bound to the β1 integrin ICD (PDB ID, 3G9W), (37), and the PTB domain of ARH bound to the LRP1 ICD (PDB ID, 3SO6) (5). In each case, $N_{-3}$ and $Y_0$ side chains from the NPxY/NxxY motif are represented in transparent green surface, and the N and C termini of the bound ICDs are indicated. (*B*) Detailed comparison of key side chains from the ICD of APP, β1 integrin, and LRP1 with respect to the SNX17 FERM domain/P-selectin complex demonstrates their similar relative orientations. All peptide side chains are colored as in *A*. The interacting side chains of SNX17 are shown as blue cylinders. (*C*) The P-selectin ICD contains overlapping Yxxϕ and NPxY/NxxY sorting motifs. The structure of the P-selectin ICD bound to SNX17 (yellow) is overlaid with the contiguous P-selectin YGVF-containing peptide bound to the AP2 μ2 subunit (magenta) (38).

cargo-binding site of the proteins also is required for their cellular localization. As shown in Fig. 4*D*, mutation of SNX27 has little effect on endosomal membrane recruitment as assessed by immunofluorescence microscopy of the protein transiently expressed in CHO cells. However, mutation of SNX17 completely abolishes the endosomal association. This result suggests that SNX17 does require membrane-coincident detection of both PI3P lipids and NPxY cargo for the formation of an organelle-specific transport complex. We speculate that the lower sensitivity of SNX27 membrane recruitment to NPxY/NxxY cargo engagement may be explained partly by an enhanced membrane affinity via additional PDZ-domain interactions with PDZbm-containing proteins.

**PX-FERM Proteins Bind Promiscuously to a Large Variety of Putative Cargos in Vitro.** The binding of SNX17 and SNX27 to several related NPxY/NxxY sequences suggests a promiscuous ability to bind signals for endosomal sorting. We thus decided to explore how widespread PX-FERM–binding signals may be by using a peptide-array screening approach and the NPxY/NxxY array originally designed to identify PTB domain-binding partners (42). Because PTB domains are known to have different specificities for phosphorylated and unphosphorylated tyrosine at the $Y_0$ position (30), both phosphorylated and unphosphorylated peptides were included on the array. GST-tagged probes of SNX17 and SNX31 and a truncated form of SNX27 (SNX27ΔPDZ) were used.

Binding to many putative cargo motifs was observed on arrays probed with the PX-FERM proteins. Importantly, SNX17 is able to bind to several known cargos such as APP and members of the LDLR family (Fig. 5) (9, 10, 13, 15, 17). The specificity of the array is further evident from the observed binding of SNX17 with peptides from integrin subunits, whereas no significant binding is observed for SNX27. This result is in agreement with siRNA-depletion assays in which an effect on trafficking of integrin subunits is observed upon SNX17 but not SNX27 depletion (11). Because our experiments demonstrate specific binding to known interaction partners, we conclude the array is also revealing interactions with previously unidentified cargo molecules.

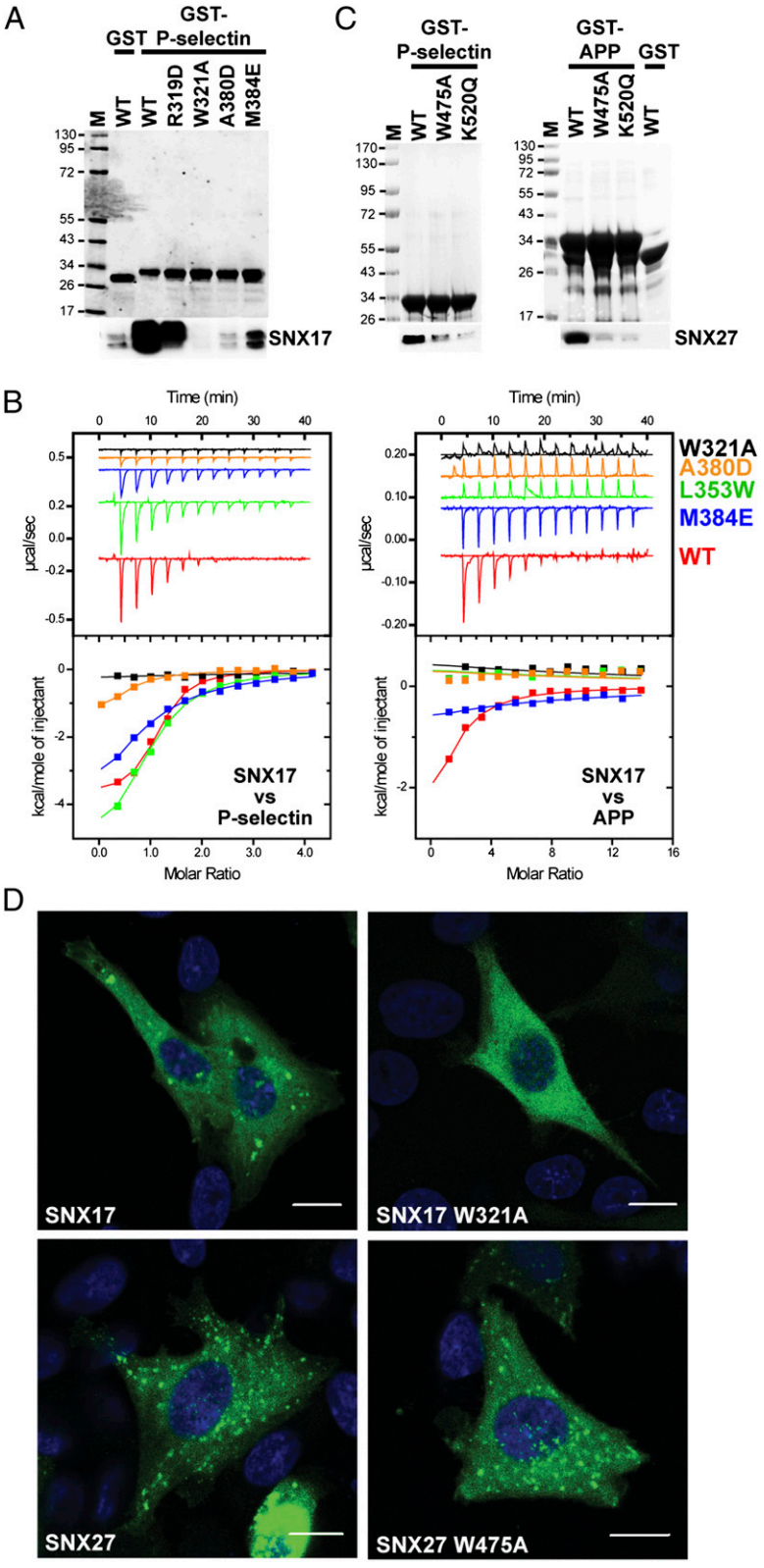


**Fig. 4.** Mutational analysis of the NPxY/NxxY cargo-binding site of PX-FERM proteins. Mutagenesis of the NPxY/NxxY-binding site of SNX17 and the analogous region of SNX27 inhibits peptide motif interactions. A full-sequence alignment of the proteins is shown in Fig. S2. (*A*) SNX17 was tested for its interaction with the GST-P-selectin ICD in GST pull-down assays. The upper panel shows the Coomassie-stained gel of the pull-down samples; the lower panel shows a Western blot using anti-His antibody to detect SNX17. (*B*) Binding of SNX17 to NPxY/NxxY motif-containing peptides derived from the ICD of P-selectin (*Left*) and APP (*Right*) was examined by ITC, using 35 μM protein and 375 μM P-selectin peptide (GTYGVFTNAAYDP) or 1 mM APP peptide (CKQNGYENPTYKFFE). Upper panels show raw data; and lower panels show integrated normalized data. (*C*) SNX27ΔPDZ was tested for its interaction with GST-APP and GST-P-selectin ICD sequences in GST pull-down assays. The upper panel shows the Coomassie-stained gel of the pull-down samples, and the lower panel shows a Western blot using anti-His antibody to detect SNX27ΔPDZ. Mutations analogous to the SNX17 motif-binding site also abolish interaction of SNX27 with the ICD sequences. (*D*) SNX17 and SNX27 were transiently expressed in CHO-InsR cells and detected by immunofluorescence labeling of the C-terminal myc tags (green). DAPI nuclear labeling is shown in blue. Both wild-type proteins show punctate endosomal recruitment, as does the SNX27 protein with an altered NPxY/NxxY-binding site (W475A mutant). The SNX17-binding mutant, however, shows a diffuse cytoplasmic distribution. (Scale bars, 10 μm.)

SNX17 shows binding to a wide variety of NPxY/NxxY peptides, suggesting that it interacts promiscuously with many different receptors, including RTKs, G-protein coupled receptors (GPCRs), integrins, LDLR, and many others (Fig. 5), and therefore may influence the trafficking and signal-transduction pathways mediated by these receptors. In addition, positive signals for the poorly characterized homolog SNX31 demonstrate that this protein also has the ability to recognize receptors in a sorting motif-dependent manner.

The SNX27 data illustrate that it also can bind to NPxY/NxxY-containing cargos from various classes. Most interestingly, SNX27 shows a significant preference for sequences that are phosphorylated

at $Y_0$, in contrast to SNX17 and SNX31, which generally show little preference. This observation suggests a potential role for SNX27 in signal activation-dependent sorting, in particular of the RTK proteins, which often contain one or more NPxY/NxxY motifs (Fig. S4) and are known to undergo extensive tyrosine phosphorylation following stimulation. To test this idea, we examined both SNX17 and SNX27 binding to two different RTKs, the insulin receptor (InsR), and the neuronal receptor TrkA (Fig. 6). It is well documented that stimulation of InsR with insulin induces phosphorylation of tyrosine residues in the NPxY motifs of the intracellular domain of the receptor (43). SNX17 and SNX27 were transiently expressed in CHO cells stably expressing InsR or in HEK293 cells transiently expressing TrkA, and the interaction was tested by immunoprecipitation both before and after stimulation with insulin or NGF, respectively. SNX17 precipitated InsR and TrkA to a similar extent before and after activation, whereas SNX27 showed a distinct preference for binding to the activated receptors. These data validate the interactions of PX-FERM proteins with RTK family members and provide some support for the contention that SNX27 can associate preferentially with receptors in an activated and phosphorylated state. Further work will be required to confirm that this association is the result of direct binding of the phosphorylated NPxY/NxxY sequences of the receptors and to determine whether similar preferences are observed for other signaling receptors.

**Model for the Coordinated Membrane and Cargo Association of PX-FERM Proteins.** Previously, using SAXS, we found that the SNX17 and SNX27 proteins have compact, globular structures in solution; however interpretation of these low-resolution data was limited by the lack of high-resolution structures of the SNX17 and SNX27 proteins for further analysis. With structures now available for the SNX27 PDZ domain (25), the SNX17 PX domain (9), and the SNX17 FERM domain (this study), we reexamined the solution structures of the proteins systematically (Fig. S5). Ab initio structures of the SNX17ΔC/P-selectin fusion protein by SAXS revealed a compact, elongated molecule. The fusion protein was used because of its greater stability during purification, and the SNX17 C-terminal tail was omitted, because it is expected to be unstructured (Fig. S2). Rigid body fitting of the two PX domain and FERM domain/P-selectin crystal structures gave a final model that showed excellent agreement with the SAXS data. The resulting structure also aligns closely with the ab initio envelopes calculated directly from the scattering data. We next performed a simple comparison of this structure with SNX27ΔPDZ, which is expected to resemble the full-length SNX17 protein (Fig. S1). Indeed we found very close agreement with the SNX27ΔPDZ scattering data without any additional rigid body refinement, implying that the common PX and FERM domains have a conserved orientation in the two proteins. Finally, this PX-FERM module was combined with the SNX27 PDZ domain (25) and rerefined as two rigid bodies against our previously measured SAXS data for full-length SNX27. The resulting model gives excellent agreement with the scattering data and confirms that the three PDZ, PX, and FERM domains form a compact, globular arrangement in solution (although a limitation of these SAXS models is that the orientations of the individual domains with respect to each other are not precisely defined).

PX-FERM proteins interact with multiple membrane-tethered ligands including NPxY/NxxY motifs, PI3P lipids, PDZbm sequences (for SNX27), and small GTPases (18), although the importance of GTPase binding in vivo remains unclear (Fig. 7). High-resolution structures now are available for each of these associated ligands except for the small GTPase proteins (9, 25); however, the recently reported structure of the Krit1 FERM domain bound to the Rap1 small GTPase (44) allows us to model with confidence how GTPase binding will occur. Structural overlay of the Krit1 FERM/Rap1 complex with the SNX17 FERM domain indicates that small GTPases from the Ras-like protein family will bind primarily to the F1 region of the PX-FERM proteins (Fig. 7). However, the overlay indicates that additional contacts will be made with the F2 region, and these contacts may help modulate binding specificity. Partial support for this notion comes from in vitro binding data showing that the F1 region alone binds to the H-Ras GTPase more weakly than does the complete SNX17 FERM domain (Fig. S6). Overlaying the high-resolution structures of the individual ligand-bound PDZ, PX, and FERM domains with the low-resolution SAXS-derived structures of SNX17 and SNX27 provides a composite model for the overall complex of the PX-FERM proteins with membrane-tethered cargo, lipids, and putative regulatory proteins, highlighting the coordinated engagement of the protein and lipid environment by these proteins at the endosome (Fig. 7).

## Discussion

PX-FERM proteins are critical regulators of recycling in the endosomal system, and here we report structural insights into the mechanism of NPxY/NxxY motif recognition by this family. Only one other structure has been solved of a sorting motif required for endosome to cell surface recycling of the SNX27 PDZ domain in complex with the Kir3.3 PDZbm (25). Overall, the

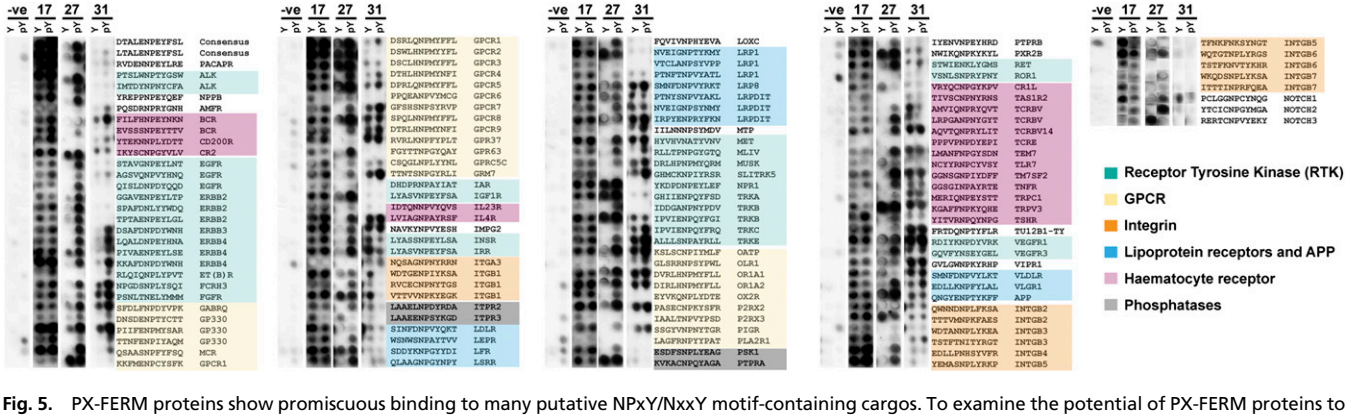


**Fig. 5.** PX-FERM proteins show promiscuous binding to many putative NPxY/NxxY motif-containing cargos. To examine the potential of PX-FERM proteins to interact with other receptors containing NPxY/NxxY, a peptide array screen was performed based on the array developed by Smith et al. (42). The arrays comprise 126 peptides derived from transmembrane proteins from the human proteome that contain NPxY/NxxY sequences and are probed in both their phosphorylated and nonphosphorylated $Y_0$ states. Cargo proteins from similar classes are highlighted. The specific constructs tested were GST-SNX17, GST-SNX31, and GST-SNX27ΔPDZ. GST alone was the negative control.

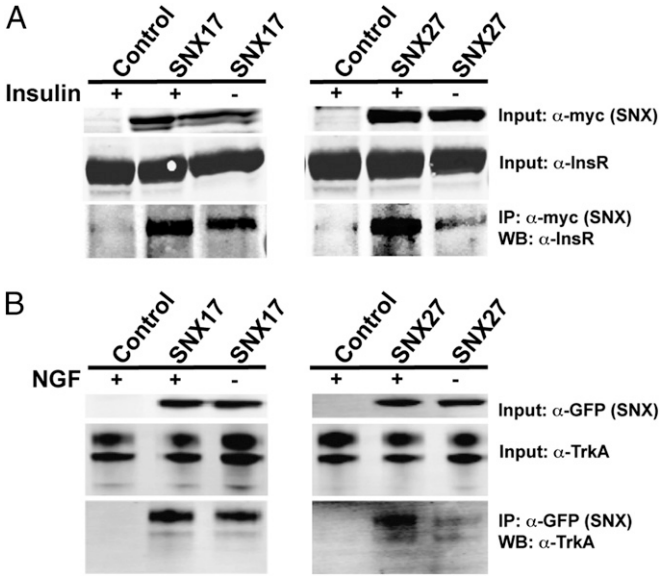


**Fig. 6.** Interaction of PX-FERM proteins with RTKs in cells. SNX17 and SNX27 with either myc or GFP tags were transiently expressed with different RTKs and tested for binding to InsR in CHO cells stably expressing the InsR (*A*) or to TrkA in transiently expressing HEK293 cells (*B*). Proteins were immunoprecipitated with indicated antibodies before and after stimulation with respective agonists, insulin (100 nM for 15 min), or NGF (3 nM for 10 min). Control experiments were performed in the absence of either SNX17 or SNX27. For TrkA experiments, proteins were crosslinked with dithiobis(succinimidylpropionate) before immunoprecipitation.

atypical SNX17 FERM domain adopts an architecture similar to the canonical FERM domains despite the unique truncated F2 subdomain, and it will be interesting to ascertain if this variation in the F2 region has a functional significance through the regulation of novel interactions. Despite the common understanding that PX domain/SNX proteins regulate membrane trafficking (18–20), only a handful of transmembrane cargos have been found to bind these proteins directly via sorting motifs within their ICDs (18). Apart from the NPxY/NxxY and PDZbm sequences recruited by the PX-FERM proteins, the only other sequences shown to bind PX proteins directly are a short stretch within the α5 integrin that interacts with nischarin (41) and a poorly defined motif in PSGL-1 that associates with SNX20 (26). Our current molecular understanding of cargo recruitment by the PX-FERM proteins thus represents an important step toward a wider comprehension of the role of PX protein family members in membrane sorting.

The structure of SNX17 in complex with the ICD of P-selectin demonstrates how a wide array of NPxY/NxxY cargos are recognized and provides a foundation for understanding how they are sorted within the endosome by the PX-FERM proteins. A summary of previously identified cargos suggests a preferred binding sequence of ϕxNPx(F/Y) (Fig. 2*A*). Notably, mouse P-selectin has an FTNAAY sequence, whereas the human P-selectin possesses an FTNAAF sequence. Although we have used the mouse P-selectin ICD in this study, it was demonstrated previously that SNX17 can interact with both human P-selectin (6) and FEEL1 (33), tolerating Phe instead of Tyr at the zero position. The cation–π interaction between the Arg319 and aromatic ring of Phe or Tyr thus appears to allow SNX17 to tolerate either of these aromatic residues. Residues upstream of the core NAAY sequence also are docked into complementary surfaces of the SNX17 protein. In particular the docking of the $F_{-5}$ residue into a hydrophobic groove capped by SNX17 Trp321 is striking, and previous mutagenesis experiments suggest that SNX17 may have a preference for binding either aromatic or bulky hydrophobic side chains at this site (6, 10, 15).

In addition to previously identified cargos, including P-selectin (6–8), APP (9, 10), integrins (11, 12), and members of the LDLR family (13–17), we have used a screening approach to identify many other putative cargo proteins for SNX17, SNX27, and SNX31. These proteins include RTKs, integrins, GPCRs, hematocyte receptors, and phosphatases, among others. Although the possibility remains to be confirmed, these results strongly suggest that PX-FERM proteins are involved in the transport of these proteins within the endosomal system. Intriguingly we find that SNX27 has a bias toward phosphorylated sorting signals and enhanced binding to at least two RTKs (InsR and TrkA) following stimulation, suggesting a possible dichotomy in the PX-FERM family by which SNX17/SNX31 and SNX27 mediate different transport itineraries depending on receptor activation states. An alternative explanation for this increased binding is that activation-dependent RTK endocytosis leads to an increased colocalization with SNX27 rather than to a direct increase in binding affinity; further studies will be necessary to differentiate

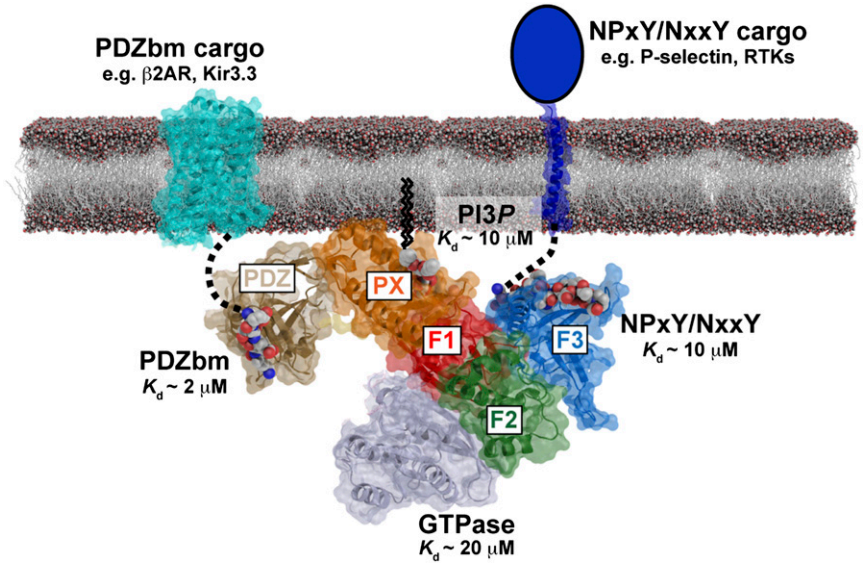


**Fig. 7.** A model for membrane-coincident binding of PX-FERM proteins to cargo, lipids, and regulatory proteins. The model shows the interaction of PX-FERM proteins with endosomal cargo (both PDZbm and NPxY/NxxY-containing molecules), the endosomal lipid PI3P, and a putative small GTPase ligand. The model is derived from the low-resolution structure of the SNX27 protein determined by SAXS (Fig. S5), overlaid with high-resolution structures of the different ligand-bound domains determined by X-ray crystallography (this study and refs. 9, 25, and 44).

between these possibilities. Although endosomal sorting clearly is an important function of the PX-FERM proteins, the finding that various signaling receptors, including RTKs and GPCRs, bind these proteins and the previous report that small GTPases also can interact (9, 45) point to an additional function in modulating endosomal signaling complexes that merits further study.

It is important to realize that NPxY/NxxY sequences are recognized within the same cargo proteins by many alternative transport adaptor and signal scaffolding proteins; for example, the LDLR receptor is recognized by ARH for internalization (5), and β integrins are bound by kindlin and talin molecules at the cell surface to regulate signal transduction (12, 27). The emerging concept of coincidence detection, as discussed here for the PX-FERM proteins, thus is critical for beginning to understand the switching between competing cytoplasmic ligands depending on their specific membrane context (Fig. 7). Because the $K_d$ for each of the individual ligands is only moderate (in the range of 1–10 μM), a coordinated interaction with the multiple membrane-tethered ligands is necessary for complex assembly; and, importantly, perturbation of only one or a small number of interactions can subsequently mediate rapid disassembly. We propose that, as the transmembrane cargos are internalized into maturing endosomal organelles, the turnover of associated proteins, and in particular membrane phosphoinositide lipids (46), will promote rapid exchange of cell-surface NPxY/NxxY-bound ligands with the endosomal PX-FERM proteins, which will assemble into stable complexes only in the presence of both PI3P and the cargo molecules themselves.

As discussed above, SNX17 promotes endosomal sorting of cargo molecules containing the NPxY/NxxY motif into Rab4-positive recycling compartments (7, 9–13, 15, 17, 33), whereas SNX27 has been found to enhance fast, Rab11-independent recycling of alternative cargo receptors via its unique N-terminal PDZ domain (22, 23). However, how this trafficking is mediated is still poorly understood, and it even has been suggested that PX-FERM proteins may not regulate active recycling but rather act indirectly to impede lysosomal degradation (12, 22). Although the recent finding that SNX27-dependent sorting may involve retromer and the WASH1 actin-remodeling complex is intriguing (22), SNX17-dependent integrin recycling does not appear to involve these molecules (11), so other components of the transport apparatus remain to be identified.

## Materials and Methods

Detailed methods are provided in *SI Materials and Methods*.

**Molecular Biology and Protein Purification.** A summary of bacterial expression constructs is given in Fig. S1. Human SNX17, mouse SNX27ΔPDZ (156–526), and mouse SNX31 were expressed in *Escherichia coli* with an N-terminal GST tag and a tobacco etch virus (TEV) cleavage site. SNX17, SNX27ΔPDZ, and SNX27-FERM (271–526) constructs were expressed with an N-terminal His tag with a TEV cleavage site. The constructs encoding SNX17ΔC (1–388) and SNX17-FERM (109–388) fused with the ICD of mouse P-selectin (residues 734–767) were expressed with an N-terminal GST tag. The ICDs of mouse P-selectin (734–767) and human APP (648 695) were expressed with N-terminal GST tags. SNX17 in pCDNA5/FRT and SNX27 in pcDNA3.1(+) were cloned for expression in mammalian cells with C-terminal myc tags. All recombinant proteins were expressed in bacteria and purified as described previously (9).

**GST Pull-Down Assays and ITC.** GST pull-down assays used 1 nmol of each GST-tagged protein and 1 nmol of either SNX17 or SNX27ΔPDZ. Pelleted proteins were washed, and bound material was analyzed by Western blot using mouse anti-His antibody. ITC experiments were performed on a Microcal iTC200 instrument in 50 mM Tris (pH 8.0), 100 mM NaCl. Peptides were titrated into SNX17 in thirteen 3.1-μL aliquots at 10 °C.

**Determination of SNX17 FERM Domain/P-Selectin ICD Crystal Structure.** The SNX17-FERM domain/P-selectin ICD chimera was crystallized in 0.1 M sodium acetate (pH 5.5), 0.2 M magnesium chloride, 15% PEG4000. For SIRAS, the crystals were soaked in 1 mM $HgCl_2$ for 10 min. Data were collected at the Australian Synchrotron MX1 beamline (Melbourne), and the phases were calculated using the peak wavelength data of Hg with AUTOSOL in the PHENIX suite. The resulting model was rebuilt with COOT (47) followed by repeated refinement and model building with PHENIX (48) and COOT (47). The final model was refined at 1.8-Å resolution. Statistics are given in Table S1.

**SAXS Data Collection and Processing.** The molar masses and monodispersity of all samples were assessed using MALLS as described previously (9) (Fig. S3; Tables S2 and S4). Homogeneous solutions of the SNX17 FERM domain fused with P-selectin ICD, SNX17ΔC fused with P-selectin ICD, the SNX27 FERM domain, and SNX27ΔPDZ were characterized using the SAXS facilities at the Australian Synchrotron (SAXS/WAXS beamline). Scattering data were background-corrected, averaged, and scaled using ScatterBrain software (written and provided by the Australian Synchrotron; available at http://www.synchrotron.org.au/), and all further processing was carried out using the ATSAS program suite (version 2.4). Ab initio free atom modeling was performed using the program GASBOR (49), and the accuracy of each model was assessed by the normalized residual coefficient, $\chi$. Low values (close to 1.0) indicate a good agreement of the models with the experimental data. Resulting models were averaged using DAMAVER (50) and filtered based on occupancy and volume to generate restored ab initio shapes of each protein. Rigid body modeling of SNX17ΔC fused with the P-selectin ICD, SNX27ΔPDZ, and full-length SNX27 was performed using BUNCH (51) with partial scattering amplitudes computed by the program CRYSOL (52). The individual rigid body domains were derived from the high-resolution crystal structures of the PX domain of SNX17 (9), the SNX17 FERM domain (this study), and the SNX27 PDZ domain (25). All SAXS data are presented according to guidelines suggested by Jacques et al. (53).

**Cell Culture, Immunofluorescence Microscopy, and Coimmunoprecipitations.** CHO cells stably expressing insulin receptor (CHO-InsR) were a kind gift from Jon Whitehead (Mater Medical Research Institute, South Brisbane, QLD, Australia) (40). Fixed and permeabilized CHO-InsR cells transfected with appropriate mammalian constructs were imaged using a Zeiss LSM 510 META confocal fluorescent microscope. For coimmunoprecipitations of InsR, CHO-InsR cells transfected with SNX27-myc or SNX17-myc were lysed, and proteins were pelleted using anti-myc antibody coupled to Protein G agarose beads as described previously (54). Samples were analyzed by Western blotting using appropriate secondary antibodies coupled to IRDye 800 or IRDye680 fluorophores, and membranes were scanned using the Odyssey infrared imaging system (LI-COR Biosciences). For insulin stimulation, cells were treated with 100 nM insulin for 15 min before lysis. For coimmunoprecipitations of TrkA, HEK293 cells were transiently cotransfected with TrkA (untagged) and SNX17-GFP or GFP-SNX27. Cells were serum starved for 3 h and subsequently treated with 3 nM NGF for 10 min before lysis. Proteins were cross-linked on ice before lysis with the membrane-permeable protein cross-linker dithiobis(succinimidylpropionate) (Pierce) and were immunoprecipitated as described previously (55).

**Peptide Array Synthesis and Analysis.** The peptide array was synthesized using N-(9-fluorenyl)methoxycarbonyl (Fmoc) chemistry on a cellulose membrane based on the SPOT technology using an auto-Spot ASP 222 Robot (Abimed). A 6-aminohexanoic acid was used as a spacer. The peptide array membrane was immersed in 100% ethanol and washed in distilled water, blocked, and then probed with 4 μM GST as negative control or with GST-tagged PX-FERM proteins in 3% BSA dissolved in blocking solution. Constructs used were GST-SNX17, GST-SNX31, and GST-SNX27ΔPDZ. Membranes were washed, probed with an anti-GST antibody in blocking solution, and developed with HRP-conjugated secondary antibody. The bound proteins were visualized by enhanced chemiluminescence.

**ACKNOWLEDGMENTS.** We thank the staff and facilities of the University of Queensland Remote Operation Crystallisation and X-ray (UQ ROCX) facility for their support; the staff of the Australian Synchrotron for assistance with X-ray diffraction; and especially Dr. Nigel Kirby for SAXS data collection. Microscopy was performed at the Australian Cancer Research Foundation (ACRF)/Institute for Molecular Bioscience Dynamic Imaging Facility for Cancer Biology, which was established with the support of the ACRF. This work was supported by Grants DP0878608 and DP120103930 from the Australian Research Council, Grants 566727 and 10012610 from the National Health and Medical Research Council (NHMRC) of Australia, and by the Canadian Cancer Society (to S.S.-C.L.). B.M.C. is supported by an Australian Research Council (ARC) Future Fellowship Award (FT100100027). E.J.C. is supported by NHMRC Career Development Award 569601. R.D.T. is supported by NHMRC Senior Research Fellowship 511042. S.S.-C.L. holds a Canadian Research Chair in Functional Genomics and Cellular Proteomics.

1. Bonifacino JS, Traub LM (2003) Signals for sorting of transmembrane proteins to endosomes and lysosomes. *Annu Rev Biochem* 72:395–447.
2. Kozik P, Francis RW, Seaman MN, Robinson MS (2010) A screen for endocytic motifs. *Traffic* 11(6):843–855.
3. Pandey KN (2010) Small peptide recognition sequence for intracellular sorting. *Curr Opin Biotechnol* 21(5):611–620.
4. Chen WJ, Goldstein JL, Brown MS (1990) NPXY, a sequence often found in cytoplasmic tails, is required for coated pit-mediated internalization of the low density lipoprotein receptor. *J Biol Chem* 265(6):3116–3123.
5. Dvir H, et al. (2012) Atomic structure of the autosomal recessive hypercholesterolemia phosphotyrosine-binding domain in complex with the LDL-receptor tail. *Proc Natl Acad Sci USA* 109(18):6916–6921.
6. Knauth P, et al. (2005) Functions of sorting nexin 17 domains and recognition motif for P-selectin trafficking. *J Mol Biol* 347(4):813–825.
7. Williams R, et al. (2004) Sorting nexin 17 accelerates internalization yet retards degradation of P-selectin. *Mol Biol Cell* 15(7):3095–3105.
8. Florian V, Schlüter T, Bohnensack R (2001) A new member of the sorting nexin family interacts with the C-terminus of P-selectin. *Biochem Biophys Res Commun* 281(4): 1045–1050.
9. Ghai R, et al. (2011) Phox homology band 4.1/ezrin/radixin/moesin-like proteins function as molecular scaffolds that interact with cargo receptors and Ras GTPases. *Proc Natl Acad Sci USA* 108(19):7763–7768.
10. Lee J, et al. (2008) Adaptor protein sorting nexin 17 regulates amyloid precursor protein trafficking and processing in the early endosomes. *J Biol Chem* 283(17): 11501–11508.
11. Steinberg F, Heesom KJ, Bass MD, Cullen PJ (2012) SNX17 protects integrins from degradation by sorting between lysosomal and recycling pathways. *J Cell Biol* 197(2): 219–230.
12. Böttcher RT, et al. (2012) Sorting nexin 17 prevents lysosomal degradation of β1 integrins by binding to the β1-integrin tail. *Nat Cell Biol* 14(6):584–592.
13. Donoso M, et al. (2009) Polarized traffic of LRP1 involves AP1B and SNX17 operating on Y-dependent sorting motifs in different pathways. *Mol Biol Cell* 20(1):481–497.
14. Betts GN, van der Geer P, Komives EA (2008) Structural and functional consequences of tyrosine phosphorylation in the LRP1 cytoplasmic domain. *J Biol Chem* 283(23): 15656–15664.
15. van Kerkhof P, et al. (2005) Sorting nexin 17 facilitates LRP recycling in the early endosome. *EMBO J* 24(16):2851–2861.
16. Burden JJ, Sun XM, García AB, Soutar AK (2004) Sorting motifs in the intracellular domain of the low density lipoprotein receptor interact with a novel domain of sorting nexin-17. *J Biol Chem* 279(16):16237–16245.
17. Stockinger W, et al. (2002) The PX-domain protein SNX17 interacts with members of the LDL receptor family and modulates endocytosis of the LDL receptor. *EMBO J* 21(16):4259–4267.
18. Teasdale RD, Collins BM (2012) Insights into the PX (phox-homology) domain and SNX (sorting nexin) protein families: Structures, functions and roles in disease. *Biochem J* 441(1):39–59.
19. Cullen PJ (2008) Endosomal sorting and signalling: An emerging role for sorting nexins. *Nat Rev Mol Cell Biol* 9(7):574–582.
20. Seet LF, Hong W (2006) The Phox (PX) domain proteins and membrane traffic. *Biochim Biophys Acta* 1761(8):878–896.
21. Hodis E, et al. (2012) A landscape of driver mutations in melanoma. *Cell* 150(2): 251–263.
22. Temkin P, et al. (2011) SNX27 mediates retromer tubule entry and endosome-to-plasma membrane trafficking of signalling receptors. *Nat Cell Biol* 13(6):715–721.
23. Lauffer BE, et al. (2010) SNX27 mediates PDZ-directed sorting from endosomes to the plasma membrane. *J Cell Biol* 190(4):565–574.
24. Lim KP, Hong W (2004) Human Nischarin/imidazoline receptor antisera-selected protein is targeted to the endosomes by a combined action of a PX domain and a coiled-coil region. *J Biol Chem* 279(52):54770–54782.
25. Balana B, et al. (2011) Mechanism underlying selective regulation of G protein-gated inwardly rectifying potassium channels by the psychostimulant-sensitive sorting nexin 27. *Proc Natl Acad Sci USA* 108(14):5831–5836.
26. Schaff UY, et al. (2008) SLIC-1/sorting nexin 20: A novel sorting nexin that directs subcellular distribution of PSGL-1. *Eur J Immunol* 38(2):550–564.
27. Elliott PR, et al. (2010) The Structure of the talin head reveals a novel extended conformation of the FERM domain. *Structure* 18(10):1289–1299.
28. Hamada K, Shimizu T, Matsui T, Tsukita S, Hakoshima T (2000) Structural basis of the membrane-targeting and unmasking mechanisms of the radixin FERM domain. *EMBO J* 19(17):4449–4462.
29. Pearson MA, Reczek D, Bretscher A, Karplus PA (2000) Structure of the ERM protein moesin reveals the FERM domain fold masked by an extended actin binding tail domain. *Cell* 101(3):259–270.
30. Uhlik MT, et al. (2005) Structural and evolutionary division of phosphotyrosine binding (PTB) domains. *J Mol Biol* 345(1):1–20.
31. Eck MJ, Dhe-Paganon S, Trüb T, Nolte RT, Shoelson SE (1996) Structure of the IRS-1 PTB domain bound to the juxtamembrane region of the insulin receptor. *Cell* 85(5): 695–705.
32. Krissinel E, Henrick K (2007) Inference of macromolecular assemblies from crystalline state. *J Mol Biol* 372(3):774–797.
33. Adachi H, Tsujimoto M (2010) Adaptor protein sorting nexin 17 interacts with the scavenger receptor FEEL-1/stabilin-1 and modulates its expression on the cell surface. *Biochim Biophys Acta* 1803(5):553–563.
34. Bergant Marušič M, Ozbun MA, Campos SK, Myers MP, Banks L (2012) Human papillomavirus L2 facilitates viral escape from late endosomes via sorting nexin 17. *Traffic* 13(3):455–467.
35. Landau M, *et al.* (2005) ConSurf 2005: The projection of evolutionary conservation scores of residues on protein structures. *Nucleic Acids Res* 33(Web Server issue):W299–302.
36. Radzimanowski J, et al. (2008) Structure of the intracellular domain of the amyloid precursor protein in complex with Fe65-PTB2. *EMBO Rep* 9(11):1134–1140.
37. Anthis NJ, et al. (2009) The structure of an integrin/talin complex reveals the basis of inside-out signal transduction. *EMBO J* 28(22):3623–3632.
38. Owen DJ, Setiadi H, Evans PR, McEver RP, Green SA (2001) A third specificity-determining site in mu 2 adaptin for sequences upstream of Yxx phi sorting motifs. *Traffic* 2(2):105–110.
39. Alahari SK, Reddig PJ, Juliano RL (2004) The integrin-binding protein Nischarin regulates cell migration by inhibiting PAK. *EMBO J* 23(14):2777–2788.
40. Thomas EC, et al. (2006) The subcellular fractionation properties and function of insulin receptor substrate-1 (IRS-1) are independent of cytoskeletal integrity. *Int J Biochem Cell Biol* 38(10):1686–1699.
41. Alahari SK, Nasrallah H (2004) A membrane proximal region of the integrin alpha5 subunit is important for its interaction with nischarin. *Biochem J* 377(Pt 2):449–457.
42. Smith MJ, Hardy WR, Murphy JM, Jones N, Pawson T (2006) Screening for PTB domain binding partners and ligand specificity using proteome-derived NPXY peptide arrays. *Mol Cell Biol* 26(22):8461–8474.
43. Kaburagi Y, et al. (1995) The role of the NPXY motif in the insulin receptor in tyrosine phosphorylation of insulin receptor substrate-1 and Shc. *Endocrinology* 136(8): 3437–3443.
44. Li X, et al. (2012) Structural basis for small G protein effector interaction of Ras-related protein 1 (Rap1) and adaptor protein Krev interaction trapped 1 (KRIT1). *J Biol Chem* 287(26):22317–22327.
45. Ghai R, Collins BM (2011) PX-FERM proteins: A link between endosomal trafficking and signaling? *Small GTPases* 2(5):259–263.
46. Cullen PJ (2011) Phosphoinositides and the regulation of tubular-based endosomal sorting. *Biochem Soc Trans* 39(4):839–850.
47. Emsley P & Cowtan K (2004) Coot: Model-building tools for molecular graphics. *Acta crystallographica. Section D, Biological crystallography* 60(Pt 12 Pt 1):2126–2132.
48. Adams PD, et al. (2010) PHENIX: A comprehensive Python-based system for macromolecular structure solution. *Acta Crystallogr D Biol Crystallogr* 66(Pt 2): 213–221.
49. Svergun DI, Petoukhov MV, Koch MH (2001) Determination of domain structure of proteins from X-ray solution scattering. *Biophys J* 80(6):2946–2953.
50. Volkov VV, Svergun DI (2003) Uniqueness of ab initio shape determination in small-angle scattering. *J Appl Cryst* 36:860–864.
51. Petoukhov MV, Svergun DI (2005) Global rigid body modeling of macromolecular complexes against small-angle scattering data. *Biophys J* 89(2):1237–1250.
52. Svergun D, Barberato C, Koch M (1995) CRYSOL - a Program to Evaluate X-ray Solution Scattering of Biological Macromolecules from Atomic Coordinates. *J Appl Cryst* 28:768–773.
53. Jacques DA, Guss JM, Svergun DI, Trewhella J (2012) Publication guidelines for structural modelling of small-angle scattering data from biomolecules in solution. *Acta Crystallogr D Biol Crystallogr* 68(Pt 6):620–626.
54. Bugarcic A, et al. (2011) Vps26A and Vps26B subunits define distinct retromer complexes. *Traffic* 12(12):1759–1773.
55. Skeldal S, et al. (2012) Mapping of the interaction site between sortilin and the p75 neurotrophin receptor reveals a regulatory role for the sortilin intracellular domain in p75 neurotrophin receptor shedding and apoptosis. *J. Biol. Chem.* 287(52):43798–43809.
56. Radzimanowski J, Beyreuther K, Sinning I, Wild K (2008) Overproduction, purification, crystallization and preliminary X-ray analysis of human Fe65-PTB2 in complex with the amyloid precursor protein intracellular domain. *Acta Crystallogr Sect F Struct Biol Cryst Commun* 64(Pt 5):409–412.